CrossMark

Effect of the graphene doping level on the electrical and optical properties of indium tin oxide (ITO) films prepared by spray pyrolysis

M.-S. Poorali[1] · M.-M. Bagheri-Mohagheghi[1,2]

Abstract A systematic study to optimize the electrical properties of ITO–graphene composite films deposited by spray pyrolysis method was investigated. The Hummers method was used for the synthesis of graphene oxide (GO) powder. Graphene was prepared by chemical reduction method from GO. To reduce GO, the most common reducing agent hydrazine hydrate at 3 ml per 100 mg of GO was used, Then, "ITO–graphene" composite films deposited by spray pyrolysis method. Structural, electrical and optical properties of films by X-ray diffraction, scanning electron microscopy, transmission electron microscopy, two-point probe method, Hall Effect experiment and UV–Vis were analyzed. The results show that graphene sheets and "ITO–graphene" composite have been produced. The obtained ITO–graphene composite films showed an energy band gap from 3.62 to 3.57 eV and sheet resistance from 7.5 to 1.5 KΩ/sq in comparison with undoped ITO films. This study showed that adding graphene to ITO film without causing much change in structural properties and energy gap, reduces the resistance of ITO film about 75 % and increases its transparency up to 90 %. The results of this study may lead to ITO–graphene composite films be more interested in sensing and solar cells applications and composites.

✉ M.-M. Bagheri-Mohagheghi
bmohagheghi@du.ac.ir

[1] School of Physics, Damghan University, Damghan, Iran

[2] P.O. Box: 91375-3889, Mashhad, Iran

1 Introduction

Graphene, a single layer of graphite, has attracted lots of attention. It has emerged in recent years as a novel and important class of materials on its own merit. This is due not only to the plethora of new fundamental science that it has displayed [1] but also to the prospect of a variety of applications that span graphene-based nano electronics devices [2], composite materials [3], and gas sensors [4] as well as energy-storage materials [5], and "paper-like" materials [6]. The remarkable properties of graphene reported so far include high values of its Young's modulus (~ 1100 GPa) [7], thermal conductivity (~ 5000 W m^{-1}K^{-1}) [8], mobility of charge carriers (200,000 cm^2 V^{-1}s^{-1}) [9] and specific surface area (calculated value, 2630 m^{2}g^{-1}) [5].

Graphene and its derivatives have unique physical and chemical properties, and have reliable synthetic methods for both solid and solution-phase processes. So graphene and its derivatives have been incorporated into a number of functional materials to composite form.

For further exploitation of these properties in various kinds of applications, versatile and reliable synthetic routes have been developed to prepare graphene and its derivatives. These methods involve bottom–up epitaxial growth [10] to the top–down exfoliation of graphite by oxidation, intercalation, and/or sonication [11]. In particular, the low-cost and mass production of chemically exfoliated GO [12] and reduced graphene oxide (RGO) sheets have been realized [13]. These products possess many reactive oxygen-containing groups for further functionalization and tuning properties of GO or reduce-GO sheets. With these added advantages, it is attractive to harness the useful properties of graphene and its derivatives in composites. This is done through the incorporation with various kinds of functional materials. Graphene and its derivatives have been used as building blocks for various kinds of

applications, including FETs [13], memories [14], photovoltaic devices [15], photocatalysis [16], sensors [17], etc.

Transparent conductive oxides (TCOs) are widely used in a variety of applications such as: optoelectronics, flat-panel displays (FPD), solar cells, gas sensors, photocatalysts, and photoelectrocatalylists and so on. Among the existing TCOs, ITO is one of the most frequently used materials, because of its unique characteristics such as good conductivity, high optical transmittance over the visible wavelength region and excellent adhesion to substrates.

ITO thin films are wide-bandgap, n-type semiconductors, which are extensively used as wave-selective coatings and mainly transparent electrodes [18]. Consequently, along with their good etch ability and adherence too many types of substrate, ITO films have become the films of choice for many applications, ranging from optical coatings to front contacts on various optoelectronic and photovoltaic devices [15].Chemical stability and photochemical properties, which originate from its n-type highly degenerate semiconductor behavior along with a wide-band gap, are other advantages of ITO films [19, 20]. ITO films can be produced by different deposition techniques, namely RTE [21], RF and DC sputtering [22], electron-beam evaporation [23] and spray pyrolysis [24]. Among the techniques currently being used, spray pyrolysis is a simple and cost-effective method. The spray pyrolysis technique is an important method for deposition of transparent conducting oxides, dielectrics, magnetic materials, and optical semiconductor thin films. It is a relatively simple and inexpensive technique for large-area coatings on glass and ceramic substrates at the atmospheric pressure.

The combination of these two materials, ITO as host material and graphene as conductive filler, with unique properties in a composite and systematic study of electrical and optical and structural properties can be considerable.

The aim of the present work is to optimize the properties of ITO using graphene. In this paper, we have systematically studied the effect of graphene on the structural, electrical and optical properties of ITO films. The deposition technique which was selected in this work was spray pyrolysis, which turned out to be a simple and cost-effective one for the deposition of good ITO films. Their morphology and microstructural characteristics were studied in detail.

2 Experimental

In the present work, at first graphene was prepared by chemical reduction of graphene oxide then five samples of ITO–graphene composite thin films were prepared by spray pyrolysis. One of them without graphene and the four other samples were prepared with different amounts of graphene as conductive filler.

2.1 Preparation of graphene

In the present work, graphene was prepared by chemical reduction method using "hydrazine hydrate" from graphene oxide. Hummers method was used for the synthesis of GO similar to the literature [25].

The chemical reduction of graphene oxide with hydrazine hydrate was performed to produce graphene according to the following steps. 100 mg of graphene oxide in 100 ml of deionized water for 1 h was dispersing.

Then 3 ml of hydrazine hydrate was added to the mixture. Mixture in an oil bath at 95 °C for 60 min in the presence of argon gas was reflux. Then, the Mixture was left black. The mixture was left overnight. Then the mixture was filtered and washed 3 times with deionized water and 3 times with ethanol, and the remaining precipitate was dried under vacuum and at room temperature for 2 h.

2.2 Preparation of thin films

ITO thin films were deposited on glass substrates using the spray pyrolysis technique. For preparation of the precursor spray solution, 3.1 mmol of indium chloride ($InCl_3$) and 0.0684 millimol of tin (IV) chloride pentahydrate ($SnCl_4$·$5H_2O$) was dissolved in 8.4 g of a solvent containing double distilled water and ethanol in a mass ratio of 1:1. To enhance the solubility of $InCl_4$, 2 ml of hydrochloric acid was also added to the solution and the solution was stirred slowly with magnetic stirring until the solution was transparent (about 15 min). The ITO film was deposited using the spray pyrolysis method. Compressed air was used as the carrier gas and 10 ml of the starting solution was sprayed on the glass substrates with a solution flow rate of 5 ml/min and a nozzle to substrate distance of 35 cm. The substrate temperature was fixed at 500 °C. Uniform coating was achieved by rotating the substrate with 30 rpm. To prepare samples ITOG25, ITOG50, ITOG75, ITOG100, respectively amount of 25, 50, 75 and 100 mg of graphene was added in the 10 ml of the precursor spray solution which was prepared in the previous step and for half an hour was dispersing. Then the process was repeated similar to the first. Deposition conditions are mentioned in Table 1.

2.3 Characterization

2.3.1 Characterization of graphene

The graphene oxide and graphene were characterized by X-ray diffraction (XRD), scanning electron microscopy

Table 1 Spray deposition parameters

Parameter	Specification
Substrate temperature (°C)	500
Solution volume (ml)	10
Solution flow rate (ml/min)	5
Nozzle to substrate distance (cm)	35
Carrier gas pressure (bar)	3
Rotating speed the substrate (rpm)	30

(SEM), and transmission electron microscopy (TEM). X-ray diffraction system (BRUKER, D8 Advance, Germany) was used for the X-ray analysis with Cu-Kα_1 radiation ($\lambda = 1.540$ Å). To know the morphology, SEM analysis was carried out for all samples. TEM images were recorded. For TEM analysis, samples were suspended in water via ultrasonication for 2 h and then the unstable dispersion was dropped on a fresh lacey carbon TEM grid.

2.3.2 Characterization of thin films

The deposited films were characterized by XRD, SEM, and electrical and optical measurements. The sheet resistance (R_S) of the films measured by two-point probe method by using thermally evaporated aluminum electrodes. The majority carrier type and carrier concentration of the films was confirmed by the Hall measurement. The Hall Effect experiment was performed at room temperature by applying a magnetic field (B = 200 mT) perpendicular to the plane of the films. The optical measurements carried out in the range of 300–1000 nm using Unico 4802 double beam spectrophotometer system.

Film thickness (t) was determined by using the optical transmission spectra (T %) and the following equation [26]:

$$t = (\lambda_1 \lambda_2)/(2n |\lambda_1 - \lambda_2|) \tag{1}$$

In which, λ_1 and λ_2 are the two consecutive peaks in transmission spectrum and n is the refractive index of glass (n $\sim$ 2). The thickness of films was $\sim$248 nm on average.

3 Results and discussion

3.1 Structural properties of graphene oxide and graphene

The graphene oxide and graphene were characterized by XRD, SEM, and TEM. XRD was used to the structural characterization of the few-layered graphene nano-sheets. We compared the structural properties of the graphene nano-sheets and GO obtained by Hummers method by

studying the powder X-ray diffraction patterns. The XRD diffraction patterns of samples are similar to previous reports [25]. Compared with pristine graphite (not shown), it can be clearly observed that the diffraction (001) peak of GO appears at $2\theta = 9.84°$. Using the Bragg equation, the distance between the plates is obtained 0.89 nm. This value is larger than the distance between graphite plates about 0.34 nm. This is due to a result of intercalation of water molecules and the formation of functional groups containing oxygen during oxidation of the graphite layers [27].

In Fig. 1, the sharp peak at $2\theta = 26.7°$ indicates a highly organized crystal structure with an d-space = 0.34 nm, which is consistent with the layer spacing of normal graphite [28]. This occurs because the interlayer spacing inside the few-layered graphene nano-sheet has a structure similar to that of normal graphite. There are rather weak peaks at about $2\theta = 9°$ in the graphene sample. This peak is similar to the typical (001) diffraction peak of GO [27], which shows more functional groups on graphene samples have been removed from the GO. Based on experimental and simulated results [29, 30], the broad peak at $2\theta = 24.7°$ can be ascribed to their few-layer nanostructures and could also be due to the complicated nature of the size, curvature, sheet rotation, and atom positioning in the graphene sheets. The broad peak at $2\theta = 20.1°$, suggests the existence of regions of expanded stacking of more corrugated or disordered graphene sheets, probably existing at the edge areas [28].

Figure 2 shows the SEM images of the graphene oxide and graphene. SEM images of GO (Fig. 2a, b) confirm the formation of layered graphene oxide structure that this sample used in the production of modified graphene
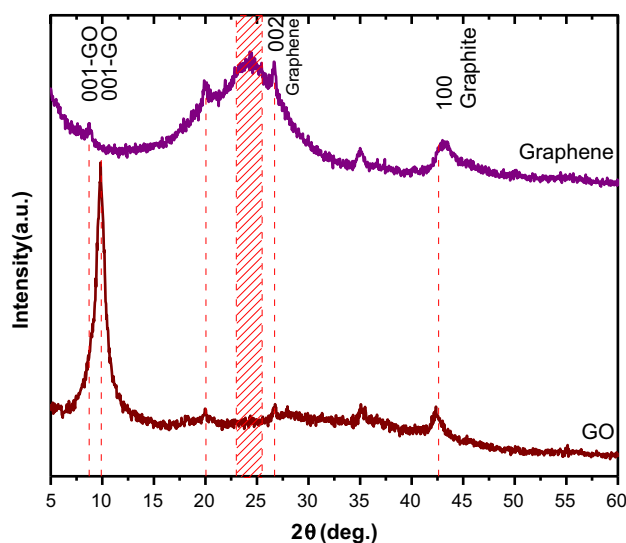

Fig. 1 XRD spectra of GO and graphene samples (1.54 Å Cu Kα_1 as wavelength)
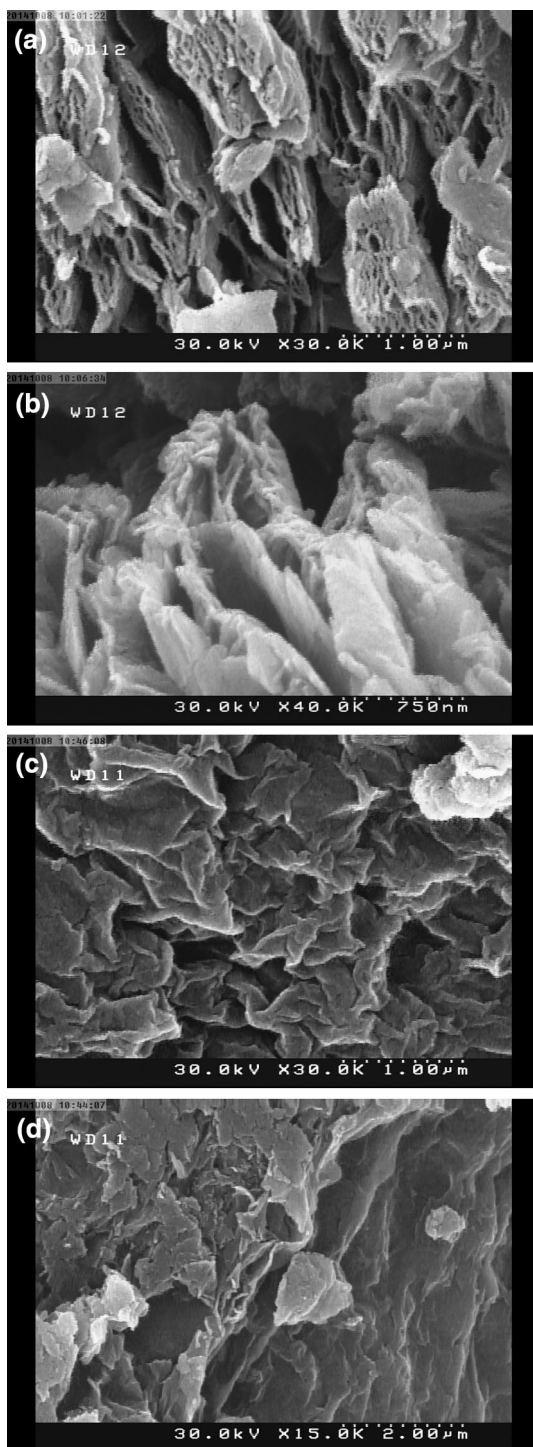
Fig. 2 SEM image at different magnifications of the **a**, **b** GO and **c**, **d** graphene

sample. Figure 2c, d shows the wrinkled structure of graphene layers.

Graphene morphology was characterized using TEM. The TEM image of sample is shown in Fig. 3. A large sheet of graphene with several hundred nanometers

dimensions found on the top of the grid, where it can be seen that there are wrinkled and transparent areas in the images. According to previous articles, wrinkled areas are part of the intrinsic nature of graphene, that becoming stable via bending [31]. It can be seen from TEM image in Fig. 3, that part of the graphene sheet shows relative flat morphology with low contrast, which is an indication of few-layer thickness. The results correspond with the results of XRD analysis. In Fig. 3, the formation of graphene sheets can be seen. Table 2 summarizes the results of the characterization of graphene.

3.2 Structural properties of ITO–graphene films

The XRD patterns of ITO–graphene films deposited on a glass substrate with different values of graphene are shown in Fig. 4. The diffraction peaks, which are related to the cubic structure of the ITO with preferred orientations in the (211), (222), (400), (440), and (622) planes, were observed at around $2\theta = 21.53°$, $30.66°$, $35.54°$, $51.10°$, and $60.71°$, respectively. The films show a polycrystalline structure with preferred orientation along the (222) plane. In Table 4, the exact location of the (222) diffraction peak of samples, Full-Width at Half Maximum (FWHM) and crystallite size (D) is listed. The crystallite size (D) is calculated using the Debye–Scherrer's formula [32]:
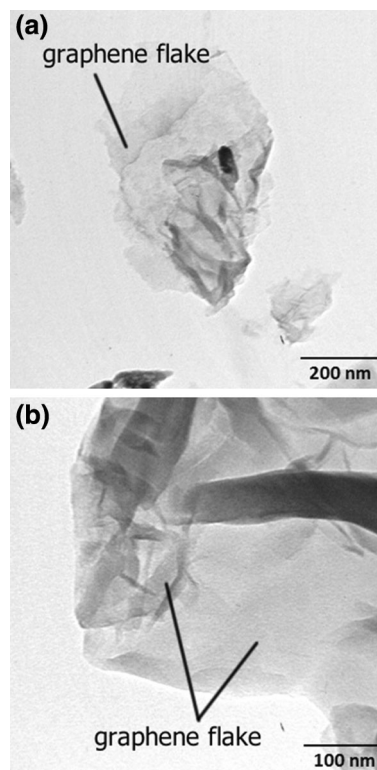
$$D = \lambda k / (\beta \cos\theta) \tag{2}$$

Fig. 3 **a**, **b** TEM image at different magnifications of the graphene

Table 2 A summary the results of the characterization of graphene

Sample	Situation	XRD	SEM	TEM
GO	Hummers method	A peak at $2\theta = 9.84°$ due to graphene oxide A peak at $2\theta = 20.1°$ due to defect in edge of area	Confirms the formation of layered graphene oxide structure	–
Graphene	Chemical reduction by 3 ml hydrazine hydrate per 100 mg GO	Remove of the GO peak at $2\theta = 9.84°$ A peak at $2\theta = 20.1°$ A peak at $2\theta = 26.7°$ due to crystal structure of graphene	Show the wrinkled structure of graphene layers	Part of the graphene sheet can be seen

Fig. 4 XRD patterns of the ITO–graphene films deposited on glass substrate for different amounts of graphene (1.54 Å Cu Kα₁ as wavelength)
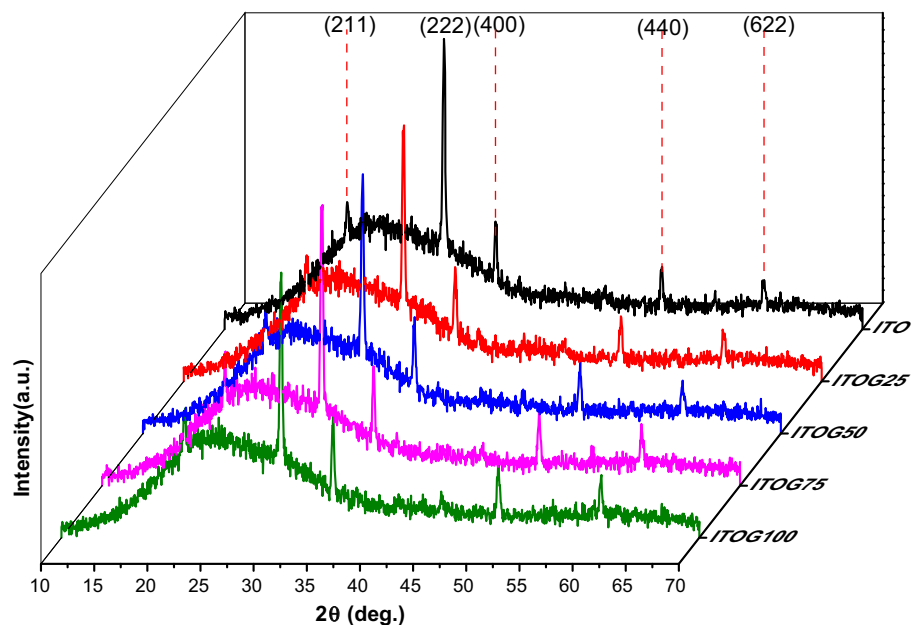
where β is the full width at half maximum of the corresponding XRD peak, k is a constant (∼1) and θ is the Bragg angle as well as λ is the wavelength of X-ray and it is 1.540 Å. The positions and shapes of the XRD peaks of ITO–graphene films remain almost the same except for the width of the peaks. As can be seen from Table 4, the FWHM value of the (222) peaks was increased from 0.24° in ITO to 0.27° in ITOG25 and ITOG75 which means reducing the size of crystalline grains. The FWHM values of the (222) peaks in ITOG50 and ITOG100 samples slightly is decreased compared to the ITO. It indicates that the degree of crystallinity in the ITO–graphene film is dependent on the amount of graphene. This can be explained by the fact that the diffusion of deposited atoms is disturbed by graphene sheets during the process.

3.3 Surface morphology of ITO–graphene films

Figure 5 shows SEM images of the samples. SEM images confirm the formation of the ITO layer in all of the cases. The micrographs show that the nanostructure of the films has a particle-cluster type growth. Almost similar morphology for samples can be seen. As can be seen graphene has an effect on aggregate. With increasing amounts of graphene, the grains have also grown.

3.4 Electrical properties of ITO–graphene films

Variations of sheet resistance (R_s) and carrier concentration (n) for all samples are shown in Fig. 6. The majority carrier concentration was calculated using the following equation by the Hall Effect measurements [32]:

Fig. 5 SEM image of the
a ITO, **b** ITOG25, **c** ITOG50,
d ITOG75 and **e** ITOG100
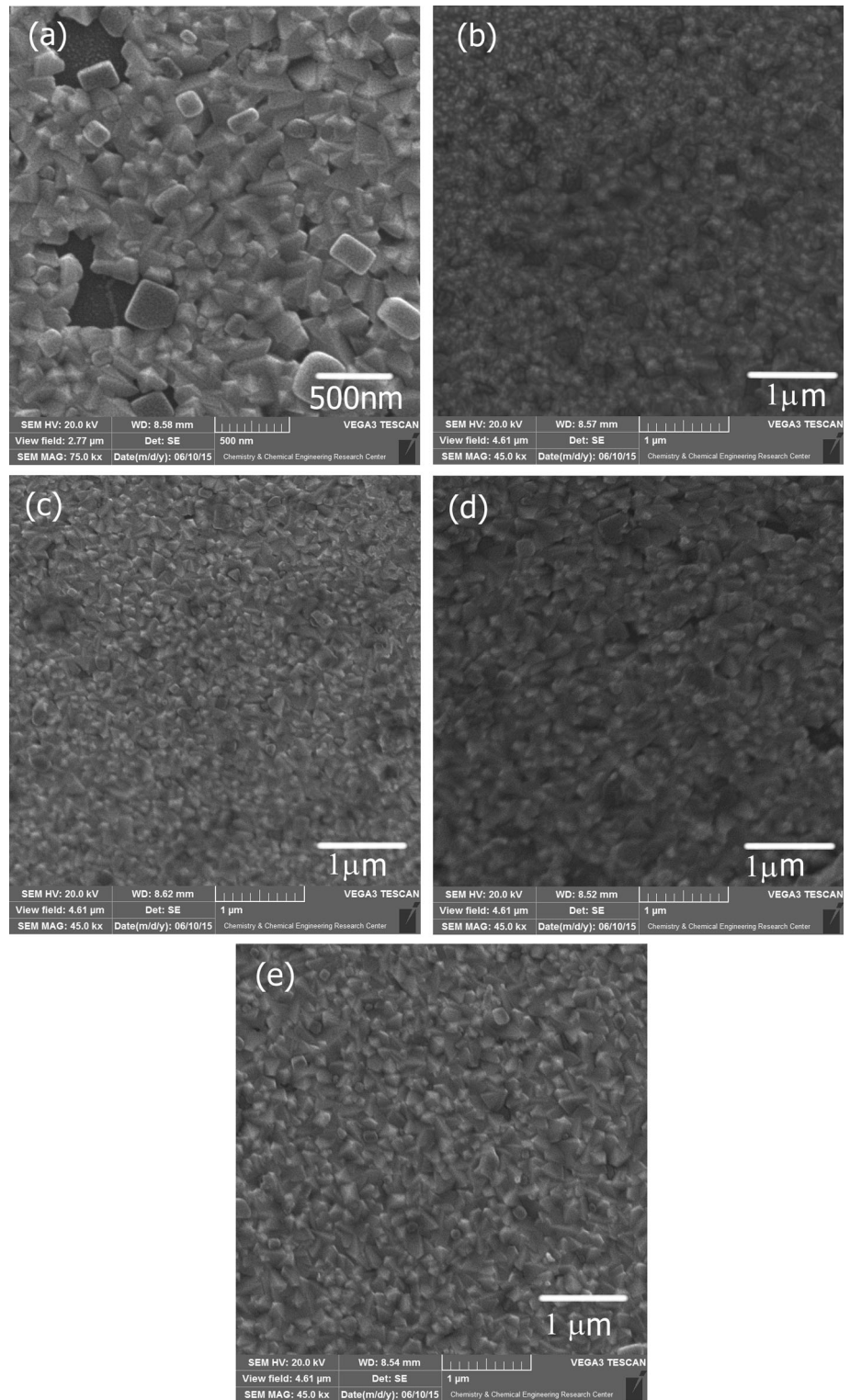
$$n = IB/(qV_H t) \tag{3}$$

In this equation, B, I, t, q and V_H are the magnetic flux density, measured current, film thickness, electron charge and Hall voltage, respectively. The Hall Effect

measurement confirms that the majority of the carriers were electrons, and the films exhibit n-type conductivity.

As it can be seen from Fig. 6, adding graphene to ITO reduces resistance layers in all cases. Resistance of the
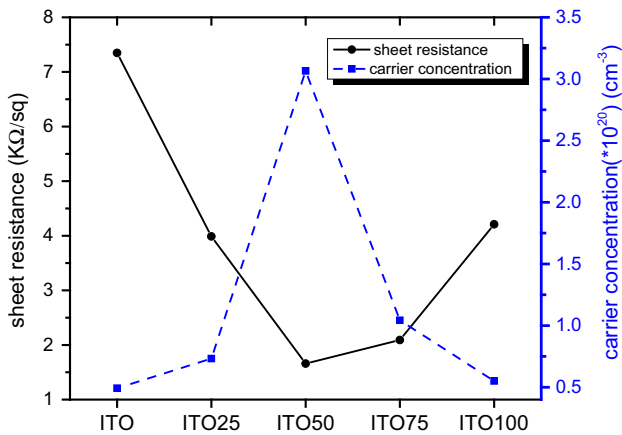
Fig. 6 Variation of sheet resistance and carrier concentration for ITO–graphene films
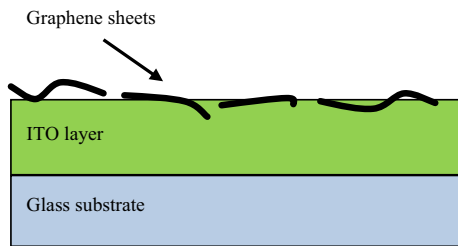

Fig. 7 A schematic view of the ITO–graphene film

ITOG25-50-75-100 ITO–graphene layers dropped 46, 77, 71 and 43 % compared to the non-graphene layer (ITO), respectively. Figure 7 is a schematic of the ITO–graphene layer. Graphene sheets during layer growth between the grains were trapped. Graphene sheets increase the conductivity of the layer. On the other hand, there is also the scattering of graphene sheet edges.

As Fig. 6 is found in the sample ITOG50, the resistance of ITO–graphene layers is optimized. Compared with non-graphene layer (ITO), resistance of layer ITOG50 has dropped more than 75 % and its sheet resistance value is approximately 1.6 kΩ/sq. This could be because the graphene sheet behaves like conductive layers and reduces resistance. With the increasing amount of graphene, scattering from defects and edges is increased and because of this resistance of the layers also increases.

3.5 Optical properties of ITO–graphene films and band gap energy estimation

The optical transmittance of the ITO–graphene films in the wavelength range of 300–1000 nm is shown in Fig. 8. It can be seen from Fig. 8 that transparency has increased. And transparency is reached from 84 % in the ITO film to
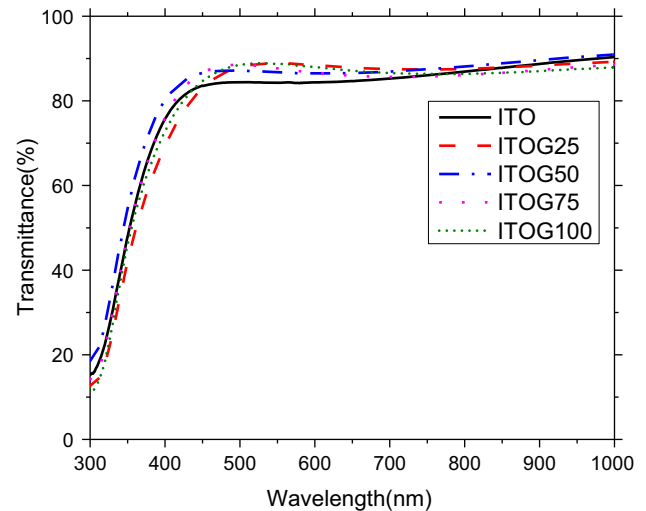

Fig. 8 Optical transmittance of ITO–graphene films

90 % in the visible region for the rest of the samples. This change occurred in transparency with regard to the same conditions of deposition for all samples. During the deposition, the only variable was the amount of used graphene. Film thickness was determined by using Eq. (1). Thickness and transmittance of each layer are shown in Table 3. As can be seen from the Table 3, using graphene changed the thickness of the layers. The thickness in samples ITOG25 and ITOG100 have grown. In the ITOG50 thickness has been reduced by 5 %. And the thickness of ITOG75 is almost not changed. Although the thickness of the layers is changed, it is significant that adding graphene reduces the transparency layer in all samples. It seems that change the transparency is due to adding graphene. This is probably due to the transparency of graphene [15].

The direct band gap (E_g) of the prepared films was obtained from the extrapolation of the linear part of the $(\alpha h\nu)^2$ curve versus photon energy ($h\nu$) and using the following equation:

$$(\alpha h\nu)^2 \propto (h\nu - E_g) \tag{4}$$

where α and E_g are the absorption coefficient and the energy gap, respectively. Figure 9 shows $(\alpha h\nu)^2$ versus $h\nu$ (photon energy) for the ITO–graphene films. The intersection of the tangent to the curve and the horizontal axis shows the gap. The values of the band gaps were obtained in the range 3.57–3.62 eV (see Table 4). The ITO film without graphene has the lowest energy gap between the other samples. Change in the energy gap of ITO film without graphene is a maximum 0.8 % in the sample ITOG100.The characterized results for ITO–graphene thin films have been summarized in Table 4.

Table 3 Thickness and transmittance of ITO–graphene composite films

Parameter	ITO	ITOG25	ITOG50	ITOG75	ITOG100
Amount of graphene (mg)[a]	0	25	50	75	100
Layer thickness (nm)	236	285	222	235	264
Transmittance	84	90	87	88	90
How to change the parameters					
The amount of used graphene	Un[b]	i[c]	i	i	i
Other deposition parameters	Un	Un	Un	Un	Un
Layer thickness	Un	i	d[d]	Un	i
Transmittance	Un	i	i	i	i

[a] In 10 ml of the precursor spray solution

[b] Unchanged compared to the ITO film [Un]

[c] The Parameter value is increased compared to the ITO film [i]

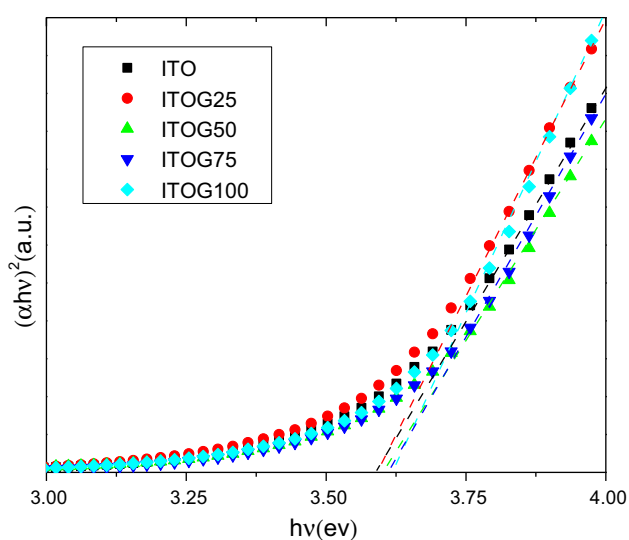[d] The Parameter value is decreased compared to the ITO film [d]

Fig. 9 Absorption curve in terms of photon energy. The intersection of the tangent to the curve and the *horizontal axis* shows the gap

4 Conclusion

A systematic approach was used to produce ITO–graphene composite films by the spray pyrolysis methods. Five samples, including ITO film without graphene and four other samples were prepared with different amounts of graphene. The structural properties and morphology of graphene were analyzed by XRD, SEM and TEM. The deposited films were characterized by XRD, SEM, and electrical and optical measurements.

Using the analysis characterized results can extract the following conclusions:

- From the TEM image shown in Fig. 3, graphene sheets have been found, where it shows transparent and rippled silk wave appearances. In accordance with the previous reported in literature, wrinkles and folded regions are part of the intrinsic nature of graphene [31]. In Fig. 3, it can be seen that the part of graphene sheet shows relative flat morphology with low contrast, indication of few-layer thickness and also obtained XRD diffraction patterns of samples are similar to previous reported [33].

- The diffraction peaks of ITO–graphene thin films are related to the cubic structure of the ITO. The films show a polycrystalline structure with preferred orientation along the (222) plane. The crystallite size (D) calculated using the Debye–Scherrer's formula demonstrates that the graphene alters the size of crystalline grains of ITO–graphene films. This is due to the fact that the diffusion of deposited atoms is disturbed by graphene sheets during the process.

- The obtained ITO–graphene films showed an electrical sheet resistance from 1.5 to 7.5 KΩ/sq. Adding graphene to ITO reduces resistance layers in all cases. Graphene sheets increase the conductivity of the layer.

- Comparison with other samples results showed that ITO–graphene composite film prepared by 50 mg graphene per10 ml of the precursor spray solution has the best electrical conductivity among other samples. Resistance of the ITOG50 dropped 77 % compared to the non-graphene layer (ITO).

- Layer transparency in the visible region increased 6 % by adding graphene to ITO films, and it reached to 90 %.Although the thickness of the layers is changed, It is significant that adding graphene reduces the transparency layer in all samples. It seems that change the transparency is due adding graphene.

- The obtained ITO–graphene films showed an energy band gap from 3.59 to 3.62 eV. Change in the energy gap of ITO film without graphene is a maximum 0.8 %. This means that graphene does not have significant effect on the electronic structure of ITO.

Table 4 A summary the results of the characterization of ITO–graphene composite films

Sample	Situation	XRD	R_S (KΩ/ sq)	Carrier concentration ($\times 10^{20}$ cm^{-3})	Transmittance in the visible range (%)	E_g (eV)
ITO	No graphene	FWHM (222) = 0.2413° in 2θ = 30.6145 (D: crystallite size = 7.414 Å	7.3	0.49	∼80	3.59
ITOG25	25 mg in 10 ml of solution	FWHM = 0.2755° 2θ = 30.6814 D = 6.4986 Å	4.0	0.73	∼90	3.59
ITOG50	50 mg in 10 ml of solution	FWHM = 0.2362° 2θ = 30.6670 D = 7.578 Å	1.7	3.06	∼90	3.60
ITOG75	75 mg in 10 ml of solution	FWHM = 0.2755° 2θ = 30.6730 D = 6.4980 Å	2.1	1.04	∼90	3.61
ITOG100	100 mg in 10 ml of solution	FWHM = 0.2362° 2θ = 30.6787 D = 7.579 Å	4.2	0.55	∼90	3.62

- Comparison of the spectra of XRD, electrical conductivity, transparency and the band gap samples show that adding graphene to ITO film (50 mg per 10 ml) without causing much change in structural properties and gap energy, reduces the resistance of ITO–graphene film about 75 % and increases its transparency up to 90 %. This method is suggested as an application method for regulation of the electrical conductivity.

- ITO–graphene composite films may be more interested in sensing and solar cells applications and composites.

References

1. A.K. Geim, K.S. Novoselov, Nat. Mater. **6**, 183 (2007)
2. G. Eda, G. Fanchini, M. Chhowalla, Nat. Nanotechnol. **3**, 270 (2008)
3. R. Verdejo, F. Barroso-Bujans, M.A. Rodríguez-Pérez, J.A. de Saja, M.A. López-Manchado, J. Mater. Chem. **18**, 2221 (2008)
4. F. Schedin, A.K. Geim, S.V. Morozov, E.W. Hill, P. Blake, M.I. Katsnelson, K.S. Novoselov, Nat. Mater. **6**, 652 (2007)
5. M.D. Stoller, S. Park, Y. Zhu, J. An, R.S. Ruoff, Nano Lett. **8**, 3498 (2008)
6. S. Park, K.-S. Lee, G. Bozoklu, W. Cai, S.T. Nguyen, R.S. Ruoff, ACS Nano **2**, 572 (2008)
7. C. Lee, X. Wei, J.W. Kysar, J. Hone, Science **321**, 385 (2008)
8. A.A. Balandin, S. Ghosh, W. Bao, I. Calizo, D. Teweldebrhan, F. Miao, C.N. Lau, Nano Lett. **8**, 902 (2008)
9. K.I. Bolotin, K.J.S. Stormer, Z.J.M. Klima, G. Fudenberg, J. Hone, P. Kim, H.L. Stormer, Solid State Commun. **146**, 351 (2008)
10. N. Xiao, X. Dong, L. Song, D. Liu, Y. Tay, S. Wu, L.-J. Li, Y. Zhao, T. Yu, H. Zhang, ACS Nano **5**, 2749 (2011)
11. X. Huang, X. Qi, F. Boey, H. Zhang, Chem. Soc. Rev. **41**, 666 (2012)
12. X. Huang, Z. Yin, S. Wu, X. Qi, Q. He, Q. Zhang, Q. Yan, F. Boey, H. Zhang, Small **7**, 1876 (2011)
13. H.G. Sudibya, Q. He, H. Zhang, P. Chen, ACS Nano **5**, 1990 (2011)
14. J. Liu, Z. Yin, X. Cao, F. Zhao, A. Lin, L. Xie, Q. Fan, F. Boey, H. Zhang, W. Huang, ACS Nano **4**, 3987 (2010)
15. Z. Yin, S. Sun, T. Salim, S. Wu, X. Huang, Q. He, Y.M. Lam, H. Zhang, ACS Nano **4**, 5263 (2010)
16. J. Du, X. Lai, N. Yang, J. Zhai, D. Kisailus, F. Su, D. Wang, L. Jiang, ACS Nano **5**, 590 (2010)
17. Z. Wang, J. Zhang, P. Chen, X. Zhou, Y. Yang, S. Wu, L. Niu, Y. Han, L. Wang, F. Boey, Biosens. Bioelectron. **26**, 3881 (2011)
18. S. Marikkannu, M. Kashif, N. Sethupathy, V.S. Vidhya, S. Piraman, A. Ayeshamariam, M. Bououdina, N.M. Ahmed, M. Jayachandran, Mater. Sci. Semicond. Process. **27**, 562 (2014)
19. C.J. Huang, Y.-K. Su, S.-L. Wu, Mater. Chem. Phys. **84**, 146 (2004)
20. B.J. Chen, X.W. Sun, B.K. Tay, Mater. Sci. Eng. B **106**, 300 (2004)
21. C.N. De Carvalho, G. Lavareda, E. Fortunato, A. Amaral, J. Non Cryst. Solids **338**, 630 (2004)
22. M. Gulen, G. Yildirim, S. Bal, A. Varilci, I. Belenli, M. Oz, J. Mater. Sci.: Mater. Electron. **24**, 467 (2013)
23. M.H. Habibi, N. Talebian, Acta Chim. Slov. **52**, 53 (2005)
24. M. Mathew, M. Gopinath, C.S. Kartha, K.P. Vijayakumar, Y. Kashiwaba, T. Abe, Sol. Energy **84**, 888 (2010)
25. M.-M. Bagheri-Mohagheghi, M.-S. Poorali, J. Mater. Sci.: Mater. Electron. **27**, 260 (2015)
26. R. Swanepoel, J. Phys. E. **17**, 896 (1984)
27. D.C. Marcano, D.V. Kosynkin, J.M. Berlin, A. Sinitskii, Z. Sun, A. Slesarev, L.B. Alemany, W. Lu, J.M. Tour, ACS Nano **4**, 4806 (2010)

28. Y. Wu, B. Wang, Y. Ma, Y. Huang, N. Li, F. Zhang, Y. Chen, Nano Res. **3**, 661 (2010)

29. Z.Q. Li, C.J. Lu, Z.P. Xia, Y. Zhou, Z. Luo, Carbon N. Y. **45**, 1686 (2007)

30. E.H.L. Falcao, R.G. Blair, J.J. Mack, L.M. Viculis, C.W. Kwon, M. Bendikov, R.B. Kaner, B.S. Dunn, F. Wudl, Carbon N. Y. **45**, 1367 (2007)

31. X. Zhang, K. Li, H. Li, J. Lu, Q. Fu, Y. Chu, Synth. Met. **193**, 132 (2014)

32. M.-M. Bagheri-Mohagheghi, N. Shahtahmasebi, M.R. Alinejad, A. Youssefi, M. Shokooh-Saremi, Solid State Sci. **11**, 233 (2009)

33. S. Dubin, S. Gilje, K. Wang, V.C.V. Tung, K. Cha, A.S. Hall, J. Farrar, R. Varshneya, Y. Yang, R.B. Kaner, ACS Nano **4**, 3845 (2010)